# Multiphysics Simulation Of An Ultrasonic Piezoelectric Motor

P. A. Carvalho[1], C. J. Nycz[1], K. Y. Gandomi[1], and G. S. Fischer[1]
[1]Robotics Engineering, Worcester Polytechnic Institute, Worcester, MA, United States

## Abstract

Operation in strong magnetic fields, vacuum or high precision positioning has often surpassed the limits of traditional actuators. Piezoelectric motors provide a suitable alternative in these applications where non-ferromagnetic based construction or low inertia may be required. We simulate and evaluate a model of an ultrasonic piezoelectric actuator. Piezoelectric simulations are inherently multiphysics; requiring both mechanical and electrical components. Ultrasonic piezoelectric motors consist of a stator with a bonded ceramic crystal and a rotor. Electrically driving the crystal through electrodes platted on its surface induce a vibration mode with a traveling wave that frictionally couples and torques the rotor. We first perform an eigenfrequency analysis of the stator structure in order to determine the resonant modes. We confirm the resonant modes with a frequency domain study. Then, we validate the motor performance through a time-domain simulation. We expect to use the results from the simulation to construct motors for driving MRI compatible surgical robots.

## Introduction

Traditional actuators can be insufficient when dealing with harsh operating conditions such as magnetic fields, hard vacuum or ultra-precision positioning. MRI compatible robots demonstrate a possible environment in which the use of traditional actuators can be undesirable due to constrained space and restriction on use of materials. Pneumatic actuators have been used to drive these robots [1, 2]. However, their slow reactions times due to long air lines can be detrimental. Hydraulic actuators such as those in [3] can be dangerous since leakages can compromise the sterile field. Piezoelectric motors such as used in [4] offer an alternative to these actuators. The low inertia of the rotor allows for fast response times and its construction can be made from nonmagnetic materials ensuring MRI compatibility.

There are several variants of piezoelectric motors; we focus on ultrasonic traveling wave resonant motors. These motors comprise of a stator and a rotor. The stator is usually composed of an aluminum or copper annular disk with ceramic elements bonded to its bottom surface. The top portion of the stator can be cut into teeth-like elements to increase its flexibility. The rotor is usually comprised of an annular aluminum disk with a bonded plastic surface. The rotor is pressed against the stator via a preloading spring. Figure 1 shows an embodiment of the construction.

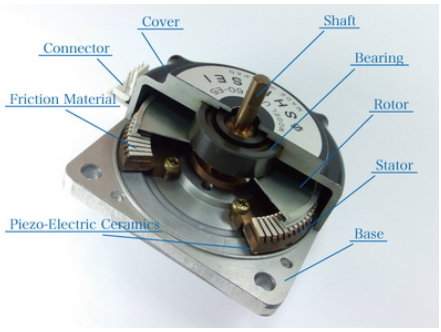


**Figure 1.** Cutaway view of a USR series Shinsei piezoelectric traveling wave motor. [5]

In this paper we extend the work of [6] by simulating a physically realizable motor based on the Shinsei Corporation USR30 (Japan) with a single mode electrode pattern that can be driven by two 90 degree shifted sine waves.

## Operating Principle

Ultrasonic motors rely on the reverse piezoelectric effect to generate motive force. This is a property that some materials exhibit in which a mechanical deformation is generated by an applied electrical field. Lead Zirconium Titanate (PZT) is one of many materials that undergo this effect and is commonly used in the construction of these motors.

A PZT ring is usually attached to the bottom of a stator with an adhesive layer of epoxy. The stator is constructed such that its relevant natural resonance modes consist of deformations in the form of tangential surface waves. We deem as relevant modes, the ones that we choose for operating the motor in. However, exciting the stator at an appropriate resonance mode is not enough for the frictionally coupled rotor to rotate. It is necessary to generate a surface traveling wave. This can be accomplished by sequentially excititing different portions of the ceramic element such that two interfering standing waves offset by $\pi/2$ in both space and phase are created. This is achievable through an appropriate electrode patterning such as in figure 2(d). A formal description of traveling waves is provided in [7].

Although the piezo ring is split into multiple sections in the model, this is not true in real motors where electric isolation and connections is done through a plated electrode over the ceramic. The blue side of figure 2(d) is the sine side whereas the red is the cosine side. In

a real motor all elements in a colored region would be shorted together with each adjacent segment polarized in an opposite direction.

## Model Setup

The USR30 stator assembly was modeled in SolidWorks 2014-2015 and imported into COMSOL 5.3a using the CAD import module. The assembly details can be seen in figure 2. A render of the stator assembly is shown in figure 3(a).

A union was created from the imported CAD model since none of the stator components move with respect to one another. Unnecessary edges were removed using virtual operations in order to avoid meshing issues. The material copper was assigned to the 47 teeth stator, epoxy was assigned to the adhesive layer and PZT-5H was assigned to the piezoceramic elements. The basic material properties can be observed in table 1. PZT-5H was used with no modification from the COMSOL material library.

The piezoelectric effect multiphysics was imported, which brings in the electrostatics and solid mechanics physics modules. Note that no electrodynamics effects are considered.

The solid mechanics module is setup to consider all components of the stator. The crystal segments are set as a piezoelectric material while all remaining parts are linear elastic materials. We setup the global coordinate system Z direction along the poling direction of the crystal which is axially up. The inner circumference of the stator hole is given a fixed constraint since it is where a nut would hold the motor into a baseplate.

The electrostatics module is setup only on the ceramic elements on the bottom of the stator. The top of the elements, which is the part that shares a boundary with the epoxy layer, is setup as ground. The bottom of each element is connected to an electric potential following the pattern outlined in figure 2(d). For the time domain simulations the potentials are in the form of equation 1 where $A$ is the driving voltage, $freq0$ is the selected simulation frequency and $t$ is the solver controlled time. Whereas for the frequency domain simulation, the potentials are described as in equation 2 where $A$ is the driving voltage and $freq$ the solver controlled frequency sweep variable. The negative of $A$ is used for the negative waves in figure 2(d) and a $\phi$, representing the phase shift, of $\pi/2$ is used for the cosine domain. A fixed driving voltage amplitude $A$ of 80V will be used throughout.

Appropriate meshing plays an important role in determining the accuracy of a finite element model simulation. The meshing used in our study can be observed in figure 3(b). The meshing parameters were set as in table 2. They were chosen as a balance between accuracy and computation time.

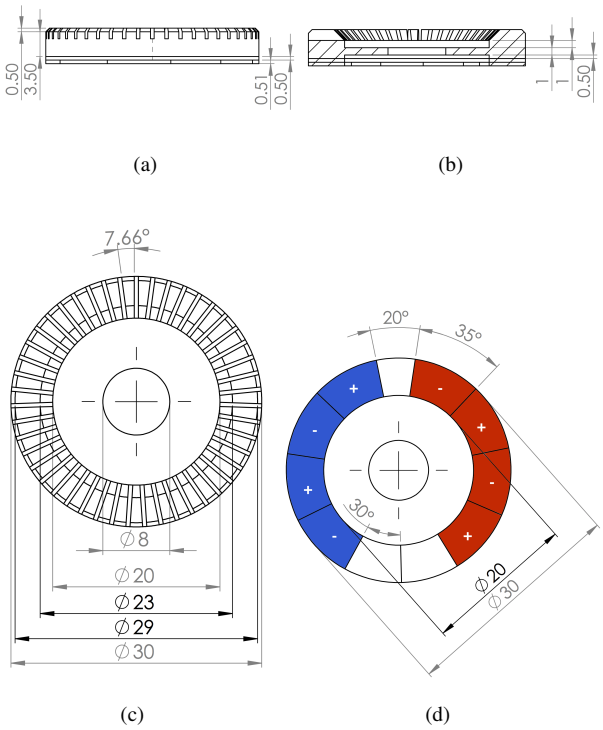


**Figure 2.** Schematic drawings of the modeled stator with bonded piezoelectric elements. (a) Side-View (b) Cutaway-View (c) Top-View (d) Bottom-View with electrode pattern.

$$A \times \sin(2 \times \pi \times freq0 \times t + \phi) \tag{1}$$

$$A \times \sin(2 \times \pi \times freq + \phi) \tag{2}$$

| Material | Density Kg/$m^3$ | Poisson's Ratio | Young's Modulus [GPa] |
|---|---|---|---|
| Copper | 8960 | 0.33 | 117 |
| Epoxy | 3500 | 0.43 | 0.7 |
| PZT-5H | 7500 | N/A | N/A |

**Table 1.** Basic material properties for the three materials used in the simulation.

| | |
|---|---|
| Max Element Size | 3 |
| Min Element Size | 0.54 |
| Max Element Growth Rate | 1.5 |
| Curvature Factor | 0.6 |
| Resolution of Narrow Regions | 0.5 |

**Table 2.** Mesh properties for stator assembly.

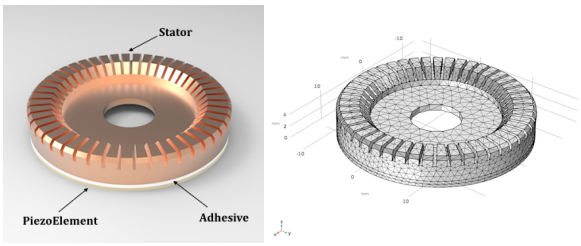


(a) (b)

**Figure 3.** (a) Render of the stator model used in simulation (b) Generated mesh of the model.

## Eigenfrequency Study

The purpose of the eigenfrequency study is to determine the resonant modes of the stator and the frequencies at which they occur. The mode corresponds to the shape that the stator will assume if driven at the particular eigenfrequency. This enables us to determine the frequencies at which we can drive the stator. Figure 4 shows the modes for the first 7 relevant eigenfrequencies. When discussing piezo motors it is often useful to describe them by their driving mode. A tenth mode motor would be one in which the mode shape contains ten peaks on its tangential surface wave. In our case, we will be operating the motor at the fifth mode for all further analysis which occurs at a driving frequency of approximately 43 kHz as observed in figure 4(e).

The eigenfrequencies provide information required for evaluating the damping coefficients that will be used in the frequency and time domain analysis. The damping ensures that the calculated magnitude values, such as displacement, more closely resemble what is expected in real life. Without damping, the time domain amplitude results would unboundedly increase over time. Note that this step would benefit from more empirical measurements but, for our purposes, we aproximated the damping with a Rayleigh model and solved for the two parameters $\beta$ and $\alpha$ using equations 3 and 4 as in [8] with the damping ratios provided in [9]. The damping coeficients were added under the linear elastic model in the solid mechanics physics as $\alpha = 352.8$ and $\beta = 6.764 \times 10^{-8}$.

$$\beta = \frac{2 \times \zeta_1 \times \omega_1 - 2 \times \zeta_m \times \omega_m}{\omega_1^2 - \omega_m^2} \tag{3}$$

$$\alpha = 2 \times \zeta_1 \times \omega_1 - \beta \times \omega_1^2 \tag{4}$$

## Frequency Domain Study

The frequency analysis will be used to demonstrate that the largest displacement of the teeth, and thus, the highest torque of the motor occurs at the resonance frequencies. These frequencies coincide with those that we computed

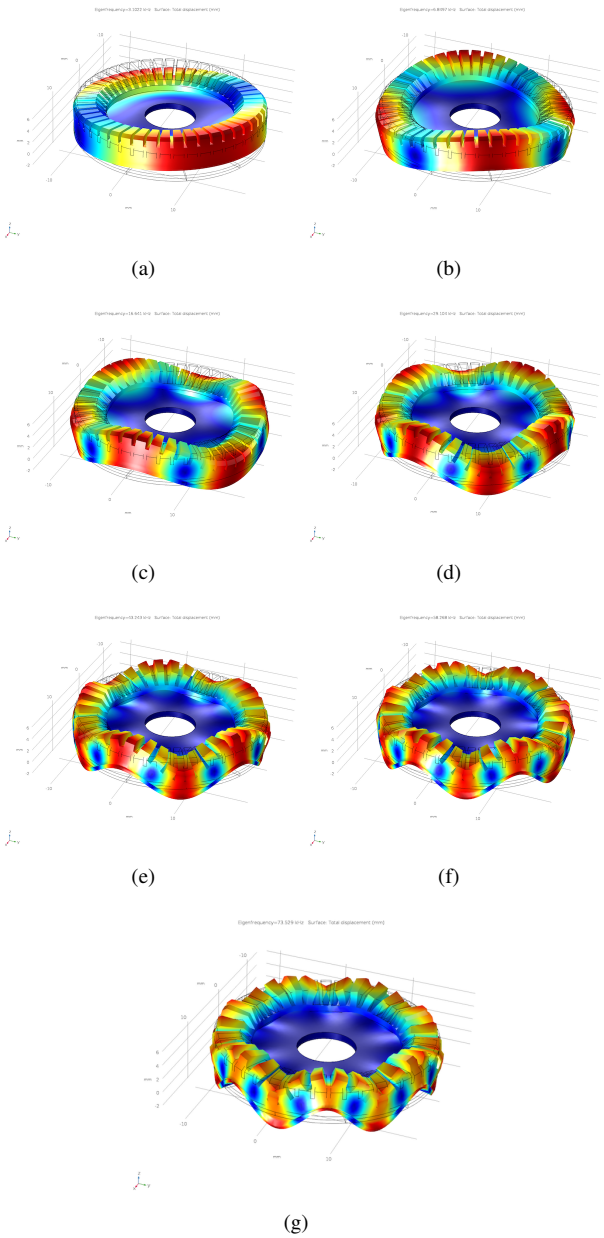

(a) (b) (c) (d) (e) (f) (g)

**Figure 4.** Results of eigenfrequency analysis searching for 40 modes around 40 kHz. Relevant results shown above. (a) Mode 1 at 3.1 kHz (b) Mode 2 at 6.9 kHz (c) Mode 3 at 16.6 kHz (d) Mode 4 at 29.1 kHz (e) Mode 5 at 43.2 kHz (f) Mode 6 at 58.3 kHz (g) Mode 7 at 73.5 kHz.

during the eigenfrequency study. Figure 5 shows the results, with a maximum overall displacement in the Z direction (perpendicular to motor) of aproximately $1.88 \mu m$. The displacement was measured with a probe placed on the top surface of one of the teeth. Note that the largest displacement does not occur in the fifth mode. However, this is acceptable since in the design of a piezoelectric motor it is important to take into account other properties such as thermal phenomena.

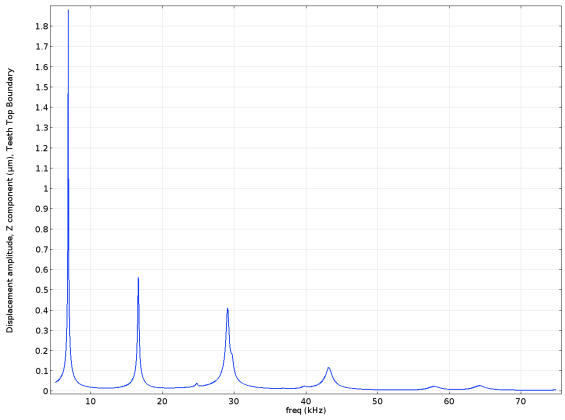


**Figure 5.** Frequency domain study results showing the resonant frequencies and corresponding amplitude displacement in the Z-direction. Frequency range from 5 KHz to 75 KHz with 20 Hz increment.

## Time Domain Study

The time domain study will compute a few important motor parameters including: Settling time and tangential velocity. The settling time was computed using a boundary probe on the top surface of one of the stator's teeth collecting Z displacement data. The results can be observed in figure 6. The motor is considered settled when the sine amplitude stops increasing. As observed, the motor settles to a steady state within 1.6ms.

The tangential velocity on the same teeth is measured with another boundary probe and can be observed in figure 7. Under the simplifying assumption that there is no slippage and contact between the rotor and stator occur at the highest extension of the teeth, the rotational speed of the motor would be given by equation 5 where $r$ is the radius and $v$ is the maximum tangential velocity. The simulated motor would therefore have a rotational speed at resonance of approximately 120rpm. The direction of rotation can be switched by changing the polarity (multiplying by $-1$) of one of the driving domains.

$$rpm = \frac{2 \times \pi \times r}{v} \tag{5}$$

## Conclusion

A multiphysics model for a piezoceramic ultrasonic resonant motor is presented. Eigenfrequency, frequency domain and time domain studies are conducted and behave as expected. Further work should include the addition of a rotor with frictional contact to the teeth such that the motor behavior can be fully explored. The damping parameters should also be evaluated more precisely and the entire model should be validated empirically through the measurement of modeled properties in a real motor.

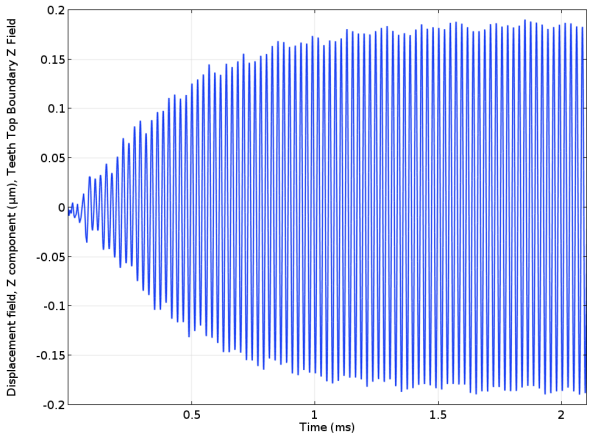


**Figure 6.** Settling time plot featuring Z displacement data versus time.

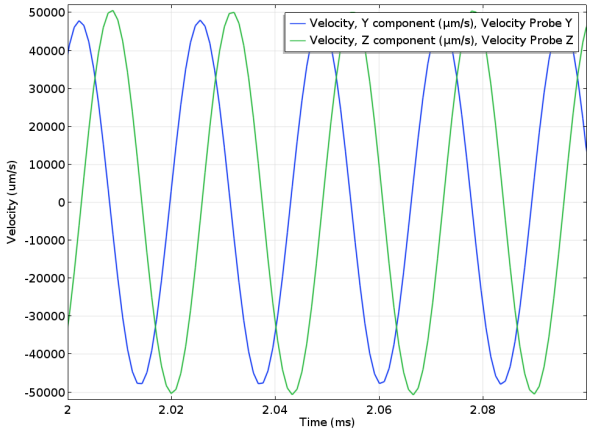


**Figure 7.** Tangential velocity of top teeth surface versus time measured by a boundary probe.

## References

1. Stoianovici, D. *et al.* "mri stealth" robot for prostate interventions. *Minim. Invasive Ther. & Allied Technol.* **16**, 241–248 (2007).

2. Fischer, G. S. *et al.* Mri-compatible pneumatic robot for transperineal prostate needle placement. *IEEE/ASME transactions on mechatronics* **13**, 295–305 (2008).

3. Kokes, R. *et al.* Towards a teleoperated needle driver robot with haptic feedback for rfa of breast tumors under continuous mri. *Med. image analysis* **13**, 445–455 (2009).

4. Nycz, C. J. *et al.* Mechanical validation of an mri compatible stereotactic neurosurgery robot in preparation for pre-clinical trials. In *Intelligent Robots and Systems (IROS), 2017 IEEE/RSJ International Conference on*, 1677–1684 (IEEE, 2017).

5. Ultrasonic motor. http://www.shinsei-motor.com/English/techno/ultrasonic_motor.html. Accessed: 2018-08-31.

6. Patel, P. & Manohar, P. Design and simulation of piezoelectric ultrasonic micro motor. *Comsol Conf.* .

7. Gabai, R. & Bucher, I. Spatial and temporal excitation to generate traveling waves in structures. *J. Appl. Mech.* **77**, 021010 (2010).

8. Chowdhury, I. & Dasgupta, S. P. Computation of rayleigh damping coefficients for large systems. *The Electron. J. Geotech. Eng.* **8**, 1–11 (2003).

9. Duan, W., Quek, S. & Wang, Q. A novel ring type ultrasonic motor with multiple wavenumbers: design, fabrication and characterization. *Smart Mater. Struct.* **18**, 125025 (2009).